Electronic Transactions on Numerical Analysis.
Volume 44, pp. 548–571, 2015.

ISSN 1068–9613.

ETNA
Kent State University
http://etna.math.kent.edu

LAMINAR-TURBULENT TRANSITION IN PIPE FLOW: WALL EFFECTS AND CRITICAL REYNOLDS NUMBER*

HIDESADA KANDA†

Abstract. This article describes possible causes of natural laminar–turbulent transition in circular pipe flow. Our starting points are the observations that under natural disturbance conditions, transition appears to take place only in the developing entrance region, as observed in Reynolds' color-band experiments, and that the critical Reynolds number R_c has a minimum value of about 2000 when using a sharp-edged uniform radius pipe, as observed in our earlier color-band experiments. The entrance region is defined as the region from the pipe inlet to the point where the inlet flow fully develops into Hagen-Poiseuille flow for a sharp-edged entrance pipe. In the case of a bell-mouth entrance pipe, the entrance region includes the bell-mouth entrance region. We derive for the entrance region a new ratio of the increase in kinetic energy flux (ΔKE flux) to a wall effect, where the wall effect is the radial wall power (R-Wall-Power) exerted on the wall by the radial component of the viscous term in the Navier-Stokes equations. In dimensionless form, ΔKE flux is a constant, although R-Wall-Power decreases as the Reynolds number Re increases. Our previous calculations for the case of a sharp-edged entrance pipe indicate that ΔKE flux $\approx$ total R-Wall-Power (T-R-Wall-Power) at Re $\approx$ 2000. Accordingly, our hypothesis is that R_c can be derived from the relation between ΔKE flux and T-R-Wall-Power. We discuss, moreover, whether or not this criterion can apply to different entrance geometries such as the bell-mouth entrances considered by Reynolds.

Key words. hydrodynamic stability, mesh refinement, thermodynamics

AMS subject classifications. 76E05, 65M50, 80A05

1. Introduction.

The notations used in this paper are given in Appendix A at the end of this paper.

1.1. The Reynolds problem.

The laminar–turbulent transition in circular pipe flow is one of the fundamental problems of fluid dynamics. In particular, a major unsolved problem is to theoretically obtain the minimum critical Reynolds number $R_{c,min} \approx 2050$, which was first observed by Osborne Reynolds in 1883 [19]. Ever since the pioneering experimental work of Reynolds, the problem has intrigued scientists, mathematicians, and engineers alike [13].

Reynolds proposed the formula Re = $\rho D V_m / \mu$, where ρ is the density, D is the circular pipe diameter, V_m is the mean axial velocity, and μ is the viscosity. He also found two critical values: an upper critical Reynolds number R_c = 12,800 by using the color-band method and a lower critical Reynolds number $R_{c,min} \approx$ 2050, which he called the real critical value, by the pressure-loss method. The precise $R_{c,min}$ value has not yet been agreed upon unanimously; it has been reported in a range from 1760 [17] to 2320 [21]. Avila et al. reported $R_{c,min}$ = 2040 $\pm$ 10 using the mean lifetime method for decaying and spreading turbulence [2]. In this present study, $R_{c,min}$ is assumed to be about 2050, as measured by Reynolds. It was furthermore observed by us in color-band experiments that under natural disturbance conditions, R_c takes a minimum value of about 2050 when using a sharp-edged entrance pipe [12].

Accordingly, in this paper, we address the following challenges as the Reynolds problems of laminar-turbulent transition in circular pipe flow:

(1) to theoretically determine a possible cause and reason why the Reynolds number itself is the primary parameter determining critical Reynolds numbers,

(2) to theoretically derive $R_{c,min} \approx 2050$, and

(3) to theoretically derive $R_c \approx 12,800$.

*Received March 14, 2015. Accepted July 17, 2017. Published online on October 9, 2015. Recommended by F. Stenger.

†Department of Computer Science and Engineering, University of Aizu, Aizu-Wakamatsu, Fukushima 965-8580, Japan (hidesada.kanda@gmail.com).

ETNA
Kent State University
http://etna.math.kent.edu

1.2. Background. The colloquium "Turbulence transition in pipe flow" was held in 2008 to commemorate the 125th anniversary of O. Reynolds' original 1883 paper. Various ongoing research topics were presented at this seminar [4]: traveling waves in pipe flow, the structure and dynamics of turbulent pipe flow, the structure of a puff, aspects of linear and nonlinear instabilities leading to transitions, the optimal path to transitions, the critical threshold in transitions, the critical layer in pipe flow, edge states intermediate between laminar and turbulent dynamics, and experiments on the decay of turbulent puffs. Then there was considerable interest in determining the mechanism of transition from laminar to turbulent flow as well as in the structure of puffs and in turbulence.

Why, however, is it difficult to solve the Reynolds problems? It seems unclear what causes all the transitions in pipe flows. Regarding the primary parameter of transition, White [27] states that "Transition depends upon many effects, e.g., wall roughness or fluctuations in the inlet stream, but the primary parameter is the Reynolds number." This gives rise to a new question: why is the Reynolds number the primary parameter determining transition to turbulence?

Regarding the effects of disturbances, Schneider and Eckhardt [22] state that "Turbulence in pipe flow has to coexist with the laminar profile since the latter is linearly stable for all Reynolds numbers. Triggering turbulence hence requires not only a sufficiently high Reynolds number but also a perturbation of sufficient amplitude. The determination of this 'double threshold' in the Reynolds number and the perturbation amplitude has been the focus of many experimental, numerical, and theoretical studies."

1.3. Possible cause and objectives. First, consider the point where transition to turbulence occurs. No transition has yet occurred in the fully developed Poiseuille region under small to medium amplitude disturbances. Thus, many researchers have stated that the flow may become turbulent long before it becomes a fully developed Poiseuille flow [7, 8, 15, 28]. Taneda [26] stated that transition in pipe flow occurs only in the entrance region.

Two causes have been proposed for transition: oscillations of disturbances and direct action of bounding walls on the flow. Most theoretical investigations of transition are concerned with stability theory based on oscillations of disturbances. However, no theory based on oscillations of disturbances yields results consistent with experimental observations such as that $R_{c,min} \approx 2050$, or about the intermittent behavior of turbulence in transition, or about the hysteresis curve of R_c (Figure 2.2).

On the other hand, Lindgren states that "the experiments indicate that real turbulence—both in flashes and in continuous turbulent regions—is maintained by direct action of the bounding walls [16]." Lindgren has investigated the relation between the wall roughness and the critical Reynolds number. In contrast, we investigate the smooth-surface wall effects on R_c.

More specifically, the present study is based on three assumptions: (a) transition to turbulence in pipe flow occurs in the entrance region, (b) possible causes of a transition process are wall effects, and (c) the type of disturbances is natural and not artificial. The results of this study will be shown to confirm assumptions (a) and (b).

The objectives of the present study are as follows:

(1) to consider the prerequisites for the transition problem associated with $R_{c,min} \approx 2050$ (Section 2),

(2) to determine a possible cause and reason why Re itself is the primary parameter determining R_c (Sections 3–6),

(3) to review our previously calculated results for $R_{c,min}$ [10] (Section 7),

(4) to discuss the differences in R_c (Section 8), and

(5) to consider the magnitude of artificial finite-amplitude disturbances (Section 9).

ETNA
Kent State University
http://etna.math.kent.edu

So far, we have obtained numerical values of 2040 and 2630 [10] for $R_{c,min}$ in pipe flow based on ideas of wall effects. This calculation method was confirmed by obtaining $R_{c,min}$ = 910 and 1230 for channel flow, where Re = HV_m/ν, H is the spacing between the parallel plates of the channel and ν is the kinematic viscosity (μ/ρ) [11].

2. Prerequisites for the transition problem.

2.1. The characteristics of R_c.

• Assumptions and quantities.

(i) The fluid is an incompressible, isothermal, Newtonian fluid with constant viscosity and density, disregarding gravity and external forces.

(ii) The fundamental quantity of laminar–turbulent transition in pipe flow is the critical Reynolds number R_c.

(iii) The Reynolds number ranges from about 1500 to about 15,000. The value of R_c depends greatly upon the experimental setup such as the use of a calming chamber, baffles, honeycomb, and screens. Accordingly, it is desirable for the initial analysis to avoid geometrically complex pipe entrances. Entrance shapes are limited to a sharp-edged entrance (St), quadrant-arc rounded entrances (Qa) cut at the pipe inlet, and bell-mouth rounded entrances (Be) as shown in Figure 2.1. Pipes have smooth-surface walls.

• Types of R_c and disturbances.

(iv) The types of disturbances are simply classified into natural (N) or artificial (A) categories. Under N-disturbance conditions, there is no artificial disturbance generator in a pipe. Under A-disturbance conditions, a disturbance generator is installed in a pipe as used in [9, 15]. The magnitudes of disturbances can be classified qualitatively but unambiguously into small (S), medium (M), or large (L) categories. For example, under N-S disturbance conditions, the fluid in a reservoir tank is kept still for at least one hour before measurement in accordance with Reynolds' color-band experiments; only then does R_c reach an upper critical Reynolds number R_{c1}. In the case of N-M disturbances, for a further example, the fluid in a tank is kept still for less than 20 minutes, and the state of the fluid in the tank is slightly disturbed, but the flow state is laminar from the inlet end to a transition point downstream as seen in our color-band experiments; the R_c type is R_{c2}. Experimental conditions of type N-L were used in Reynolds' pressure-drop experiments, where he used a valve arranged at some distance upstream from the pipe inlet. The flow state was turbulent from the valve, and the type of transition was turbulent to laminar flow (reverse transition); the R_c type is R_{c3}.

(v) Each experimental apparatus has two critical Reynolds numbers: R_{c1} and R_{c2}. R_{c3} is assumed to be about 2050 regardless of the apparatus.

• R_c and transition process.

(vi) Transition takes place by the appearance of an increasing number of turbulent flashes for increasing Re [16, 19]; R_{c1} is assumed to be the Reynolds number at which turbulent flashes first appear. R_{c2} and R_{c3} are the Reynolds numbers at which a laminar color-band recovers from a disturbed turbulent state.

(vii) The transition process must be the same for pipe and channel flows since there exists $R_{c,min}$ for both, respectively. In contrast, there is no $R_{c,min}$ for flow on a flat plate, so that the transition process for flow on a flat plate is different from those for pipe and channel flows.

2.2. The minimum critical Reynolds number. Let us review the results of our earlier color-band experiments. Figure 2.1 (cf. [12, Figure 3]) shows the bell-mouth and quadrant-arc rounded entrances of a test pipe of 2.6 cm diameter and about 155 cm length, along with the experimental results for R_{c1} and R_{c2}. Figure 2.2 (cf. [12, Figure 5]) shows the values of R_{c1} and R_{c2} plotted against the contraction ratio C_b of the quadrant-arc entrance and the bell-mouth entrance diameters to the pipe diameter.

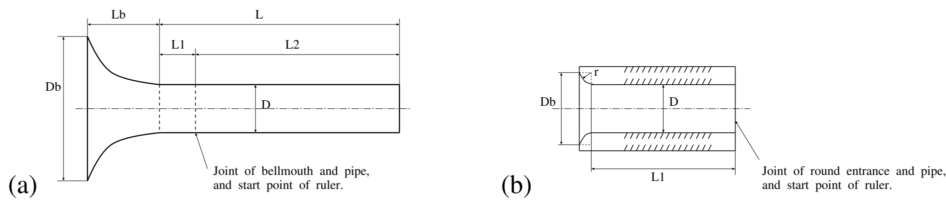

Entrance	D_b	r	L_b	C_b	R_{c1}	R_{c2}
St	2.6	0.0	-	1	2200	2050
Qa1	2.8	0.1	0.1	1.08	3600	3150
Qa2	3.0	0.2	0.2	1.15	5000	4100
Qa3	3.2	0.3	0.3	1.23	6700	4650
Qa4	3.4	0.4	0.4	1.31	8750	4850
Qa5	3.6	0.5	0.5	1.39	12,200	5200
Be1	4.0	-	1.05	1.54	12,500	5200
Be2	6.07	-	2.6	2.34	12,200	5450
Be3	10.4	-	5.85	4	12,500	5500
Be4	15.6	-	9.75	6	12,200	5500

FIG. 2.1. *(a) Bell-mouth entrance and (b) quadrant-arc entrance. Sizes of ten pipe entrance shapes ($D = 2.6$ cm, L2 = 150 cm), and experimental results for R_{c1} and R_{c2}; cf. [12, Figure 3 and Table 6].*

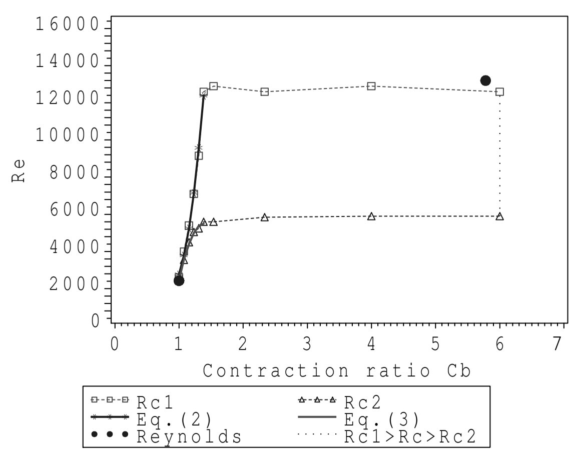

FIG. 2.2. *Hysteresis curve drawn by connecting two sequences of R_{c1} and R_{c2} plotted against C_b; cf. [12, Figure 5].*

From Figure 2.2, it can be seen that both R_{c1} and R_{c2} are almost completely determined by the small radius of the quadrant-arc rounded entrance (r = 1–5 mm). The values of R_{c1} and R_{c2} increase steadily and smoothly as C_b increases from 1 (St) to 1.39 (Qa5), and then R_{c1} and R_{c2} reach approximately constant values of 12,200–12,500 and 5200–5500, respectively. The minimum values of $R_{c1,min}$ = 2200 and $R_{c2,min}$ = 2050 were obtained with a sharp-edged circular pipe. Therefore, the minimum critical Reynolds number of $R_{c,min} \approx 2050$ was observed for $R_{c2,min}$ [12] and $R_{c3,min}$ [19].

• Vena contracta.

Flow through a sharp-edged corner is characterized in general by a convergence of streamlines in the vicinity of the inlet. At some location downstream of the inlet, however, the streamlines again can be considered parallel, and the flow area at this location (called the vena

ETNA
Kent State University
http://etna.math.kent.edu

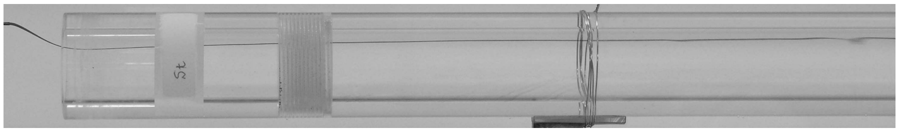

FIG. 2.3. *No vena contracta at a sharp edged entrance in our color band experiment, and a turbulent flash at 29.5 cm downstream from the inlet end (top right position in the picture), Re = 2265.*

contracta) is found in general to be less than that at the geometric opening of the pipe inlet [3]. Fox and McDonald [5] state that "If the inlet has sharp corners, flow separation occurs at the corners, and a vena contracta is formed. The fluid must accelerate locally to pass through the reduced flow area at the vena contracta."

In contrast, however, in our color-band experiments, neither a vena contracta nor an inflection point were observed at the sharp-edged inlet corner, as shown in Figure 2.3, where Re = 2265. The fluid entered the pipe smoothly, and a turbulent spot suddenly appeared 29.5 cm downstream from the pipe inlet. Similarly, another pipe inlet flow observed experimentally appeared not to have an inflection point at its sharp-edged corner. We thus conclude that the vena contracta is negligible in color-band experiments using a sharp-edged pipe in a large water tank.

2.3. Entrance length. The entrance region considered in this study includes bell-mouth entrances. Thus, the inlet ($x = 0$) is the pipe inlet for a sharp-edged entrance pipe and is the bell-mouth inlet end for bell-mouth entrance pipes. The entrance length x_e is defined as the distance from the inlet to the point downstream where the center-line velocity u_c reaches 99% of its fully developed value ($u_c/V_m = 1.98$). Then, the dimensionless entrance length L_e is given [23] by

$$L_e = \frac{x_e}{D\,\mathrm{Re}} = 0.056, \qquad \mathrm{Re} \geq 500, \tag{2.1}$$

while L_e for u_c reaching 99.9% of its fully developed value is 0.075 [23]. Since the bell-mouth axial length is small, L_e in (2.1) can be used both for sharp-edged pipes and for bell-mouth entrance pipes.

2.4. Transition length. Reynolds [19] states that "Under no circumstances would the disturbance occur nearer to the trumpet than about 30 diameters in any of the pipes, and the flashes generally but not always commenced at about this distance." Reynolds used three straight circular pipes in his color-band experiments. Their diameters were D = 0.7886, 1.527, and 2.68 cm, and their length x_p was nearly 5 feet (152 cm) giving dimensionless pipe lengths x_p/D of 193, 100, and 57, respectively. Let us consider the transition length x_t. The dimensionless transition length L_t is defined as the normalized distance from the inlet to the point where transition to turbulence takes place,

$$L_t = \frac{x_t}{D\,\mathrm{Re}}\,.$$

In Reynolds' color-band experiments, x_t was more than $30D$, but it should be less than the pipe length 152 cm. Accordingly, for the pipe with D = 2.68 cm, the transition length is bounded at Re = 12,800, so that

$$30D < x_t < 57D \qquad \text{and} \qquad 0.00234 < L_t < 0.00445.$$

Consider now our experimental results for the transition length. For the sharp-edged pipe, under N-S disturbance conditions, x_t ranged from about $7D$ (L_t = 7/2265 = 0.0031) to

ETNA
Kent State University
http://etna.math.kent.edu

$20D$ (L_t = 20/2250 = 0.0089). Under N-M disturbance conditions, x_t ranged from about $4D$ (L_t = 4/2160 = 0.0019) to $22.3D$ (L_t = 22.3/2020 = 0.0110). The transition lengths under N-S and N-M disturbance conditions are approximately the same. Moreover, for the Be4 bell-mouth entrance, corresponding to Reynolds' bell-mouth with C_b = 6 (pipe of D = 2.68 cm), under N-S disturbance conditions, x_t ranged from about $19D$ (L_t = 19/11590 = 0.0016) to $54D$ (L_t = 54/11060 = 0.0049) for $R_t \approx$ 10,000–13,700. These results approximately agree with Reynolds' observation of $x_t > 30D$.

In short, under N-S or N-M disturbance conditions, natural transition to turbulence seems to occur only in the entrance region, particularly in the vicinity of the pipe inlet, but does not occur at the pipe inlet itself.

2.5. Pressure drop in the entrance region. Here the pressure difference and the pressure drop are defined and distinguished to avoid confusing them. Let the pressure at the inlet ($x = 0, i = 1$, see Figure 2.4) be zero.

(i) The axial pressure difference $(\mathit{\Delta} p)_x$ is negative, defined as

$$(\mathit{\Delta} p)_x \equiv p(x + \mathit{\Delta} x) - p(x) = p_{i+1} - p_i < 0,$$

and can be used in finite difference expressions, i.e.,

$$\frac{\partial p}{\partial x} \approx \frac{(\mathit{\Delta} p)_x}{\mathit{\Delta} x} .$$

(ii) The axial pressure drop is positive and usually defined as

$$\mathit{\Delta}\mathcal{P}(x) = p(0) - p(x) = 0 - p(x) = -p(x) > 0.$$

(iii) There is a significant radial pressure drop $(\mathit{\Delta} p)_{wc}$ in the radial direction between the pressure on the wall ($p_w = p|_{r=R}$) and the pressure on the centerline ($p_c = p|_{r=0}$) (see Figure 7.2):

$$(\mathit{\Delta} p)_{wc} = p_w - p_c < 0.$$

Note that $(\mathit{\Delta} p)_{wc}$ cannot be disregarded, whereas the boundary-layer approximations disregard this radial pressure drop.

(iv) The total pressure drop $\mathit{\Delta}\mathcal{P}$ from the pipe inlet consists of two components: (a) the pressure drop based on the fully developed flow, $f(x/D)$, and (b) an additional pressure drop $K(x)$ due to a momentum change $\mathit{\Delta}$KE flux(x) and an accumulated increment in the wall shear $K_{\text{Shear}}(x)$ between developing flow and Poiseuille flow [23]; i.e., $K(x) = \mathit{\Delta}\text{KE flux}(x) + K_{\text{Shear}}(x)$. Accordingly, $\mathit{\Delta}\mathcal{P}$ is expressed as

$$\mathit{\Delta}\mathcal{P}(x) = \left(f\frac{x}{D} + \mathit{\Delta}\text{KE flux}'(x) + K_{\text{Shear}}(x)\right)\left(\frac{1}{2}\rho V_m^2\right) > 0, \tag{2.2}$$

where the Darcy-Weisbach friction factor f is $64/\text{Re}$ for Poiseuille flow (see (6.10)), and a prime ' denotes a dimensionless variable; see (6.4). When using the dimensionless axial coordinate $X = x/(D\text{Re})$, (2.2) is not a function of Re and can be expressed as

$$\mathit{\Delta}\mathcal{P}(X) = \left(64X + \mathit{\Delta}\text{KE flux}'(X) + K_{\text{Shear}}(X)\right)\left(\frac{1}{2}\rho V_m^2\right) > 0.$$

$K(x)$ increases monotonically from 0 at $x = 0$ to a constant value $K(\infty)$ in the fully developed region, and the experimental value of $K(\infty)$ is reported as varying from 1.20 to 1.32 [23]. Note that $K(\infty)$ includes an $\mathit{\Delta}$KE flux$'$ of about 1 (see (6.4) and (6.6)), which is the increase in kinetic energy flux from the entrance flow to Hagen-Poiseuille flow.

ETNA
Kent State University
http://etna.math.kent.edu

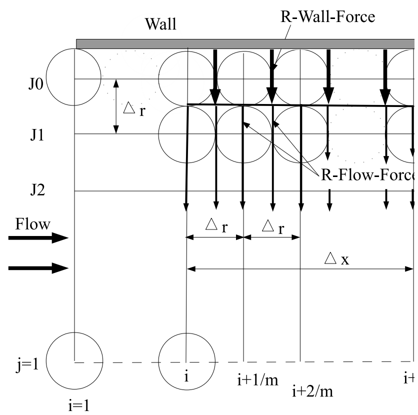

FIG. 2.4. *Mesh system with radial wall force and radial flow force.*

3. Wall effects and pressure.

3.1. The wall model.

(i) What are wall effects for determining R_c? We consider why the transition between laminar and turbulent flow occurs in circular pipes with smooth-surface walls. Roughness effects of pipe wall surfaces on R_c are excluded in this study.

Panton [18] states about a wall model that "the no-slip condition at the wall means that the particles are not translating; however they are undergoing a rotation. We might imagine that the wall consists of an array of marbles, which are rotating but remain at the same location on the wall."

In Figure 2.4, the vorticities on the wall ($j = J0, r = R - (1/2)\Delta r \approx R$) are fixed and rotating but are not moving downstream. We assume that the wall effects are due to forces, work, energies, and power acting upon fluids by the vorticities on the wall.

(ii) Since axial and radial velocities on the wall are zero, the vorticity on the wall in two dimensions is defined by

$$\omega_\theta|_{r=R} \equiv \frac{\partial v}{\partial x} - \frac{\partial u}{\partial r} = -\frac{\partial u}{\partial r} = -\frac{du}{dr}\,. \tag{3.1}$$

Differentiating (3.1) with respect to r gives

$$\left.\frac{d\omega_\theta}{dr}\right|_{r=R} = -\frac{d^2u}{dr^2}\,. \tag{3.2}$$

(iii) The Navier-Stokes equation in vector form is expressed as

$$\rho\left(\frac{\partial V}{\partial t} - V \times \omega\right) = -\nabla\left(p + \frac{1}{2}\rho V^2\right) - \mu\nabla \times \omega, \tag{3.3}$$

where V is the velocity vector and p is the difference of the actual pressure from the hydrostatic [6].

Since $V = 0$ on the wall, (3.3) reduces to

$$-\mu(\nabla \times \omega)|_{r=R} = \nabla p < 0.$$

ETNA
Kent State University
http://etna.math.kent.edu

The axial component of the curl of vorticity in two dimensions is expressed from its definition:

$$
\begin{aligned}
-\mu(\nabla\times\omega)_x|_{r=R} &\equiv -\mu\frac{1}{r}\left[\frac{\partial}{\partial r}(r\omega_\theta)-\frac{\partial\omega_r}{\partial\theta}\right] = -\mu\frac{1}{r}\frac{\partial}{\partial r}(r\omega_\theta)\\
&= -\mu\left(\frac{\partial\omega_\theta}{\partial r}+\frac{\omega_\theta}{r}\right) = \frac{\partial p}{\partial x} < 0.
\end{aligned}
\tag{3.4}
$$

Similarly, the radial component of the curl of vorticity is given from its definition:

$$
-\mu(\nabla\times\omega)_r|_{r=R} \equiv -\mu\left(\frac{1}{r}\frac{\partial\omega_x}{\partial\theta}-\frac{\partial\omega_\theta}{\partial x}\right) = \mu\frac{\partial\omega_\theta}{\partial x} = \frac{\partial p}{\partial r} < 0.
\tag{3.5}
$$

Hereafter, ω denotes ω_θ since ω_r and ω_x vanish in two dimensions.

4. Axial force and power. In this section, we consider axial forces and powers in the fully developed Poiseuille region.

4.1. Axial wall and flow forces.

(i) By the wall we mean the fluid particles on the wall [18]. Equation (3.4) indicates that a negative force in the axial direction is active on the wall by a rotation of the particles resulting in an axial pressure difference or an axial pressure drop.

(ii) The wall shear τ_w is expressed as

$$
\tau_w = \mu\left.\frac{du}{dr}\right|_{r=R} < 0.
\tag{4.1}
$$

The applied forces due to the wall shear τ_w and the axial pressure difference $(\varDelta p)_x$ for the axial small distance $\varDelta x$ are related [27] as

$$
2\pi R(\varDelta x)\tau_w = \pi R^2(\varDelta p)_x < 0,
\tag{4.2}
$$

where R is the pipe radius. Equation (4.2) shows that the wall shear on the wall equals the pressure difference in the axial direction in a fluid.

Using (3.4) and (4.2), the wall shear can be expressed from the axial component of the curl of vorticity as

$$
\tau_w = -\left.\frac{1}{2}\mu R(\nabla\times\omega)_x\right|_{r=R} = -\frac{1}{2}\mu R\left(\frac{\partial\omega_\theta}{\partial r}+\frac{\omega_\theta}{r}\right) = \frac{1}{2}R\frac{\partial p}{\partial x}\cdot
\tag{4.3}
$$

(iii) We confirm (4.3) in Hagen-Poiseuille flow, where the axial velocity distribution u is

$$
u = 2V_m\left[1-\left(\frac{r}{R}\right)^2\right].
\tag{4.4}
$$

Differentiating (4.4) with respect to r on the wall gives

$$
\left.\frac{du}{dr}\right|_{r=R} = -\frac{4V_m}{R} \quad\text{and}\quad \left.\frac{d^2u}{dr^2}\right|_{r=R} = -\frac{4V_m}{R^2}\cdot
\tag{4.5}
$$

From (3.1), (3.2), and (4.5), we have

$$
\omega|_{r=R} = -\left.\frac{du}{dr}\right|_{r=R} = \frac{4V_m}{R} = -R\left.\frac{d^2u}{dr^2}\right|_{r=R} = R\frac{d\omega}{dr}\cdot
\tag{4.6}
$$

From (4.1) and (4.6), the wall shear is expressed as

$$\tau_w = \mu \left.\frac{du}{dr}\right|_{r=R} = -\mu\, \omega|_{r=R} = -\mu R\frac{d\omega}{dr} = -\frac{4\mu V_m}{R}. \tag{4.7}$$

Accordingly, the axial viscous term of the N-S equations is expressed from (3.4), (4.6), and (4.7) as

$$\begin{aligned} -\mu R\,(\nabla\times\omega)_x|_{r=R} &= -\mu R\left(\frac{d\omega}{dr}+\frac{\omega}{r}\right) = -\mu R\left(\frac{4V_m}{R^2}+\frac{4V_m}{R^2}\right)\\ &= -\frac{8\mu V_m}{R} = 2\tau_w. \end{aligned} \tag{4.8}$$

Thus (4.3) is confirmed for Hagen-Poiseuille flow by (4.8). It is clear that the wall shear or the axial component of the curl of vorticities on the wall is one of the wall effects.

(iv) The left-hand and right-hand terms in equation (4.2) can be called A-Wall-Force and A-Flow-Force, respectively.

$$\begin{aligned} \text{A-Wall-Force} &= 2\pi R(\mathit{\Delta} x)\tau_w = 2\pi R(\mathit{\Delta} x)\left[-\frac{1}{2}\mu R(\nabla\times\omega)_x\right]_{r=R}\\ &= -\pi\mu R^2(\mathit{\Delta} x)\,(\nabla\times\omega)_x|_{r=R} = -\mu\mathcal{V}\,(\nabla\times\omega)_x|_{r=R} < 0, \end{aligned} \tag{4.9}$$

and

$$\text{A-Flow-Force} = \pi R^2(\mathit{\Delta} p)_x < 0,$$

where $\mathcal{V}$ is the volume for the axial distance $\mathit{\Delta} x$ in a pipe.

(v) Note that A-Wall-Force on the wall exerts an equal force A-Flow-Force on a fluid in the axial direction by Newton's Second Law of Motion.

(vi) Regarding $(1/2)R$ in (4.3), it is noted from (4.9) that $2\pi R\mathit{\Delta} x \times (1/2)R = \mathcal{V}$, i.e., the wall surface exerts $\mu(\nabla\times\omega)_x|_{r=R}$ on all the fluids for $\mathit{\Delta} x$ in a pipe.

4.2. Axial wall and flow powers. A-Wall-Force does negative work on fluids on the wall resulting in a pressure difference in the axial direction in a fluid. This negative work can be called the axial wall power (A-Wall-Power), and the energy loss of the fluid is called the axial flow power (A-Flow-Power) since their physical dimension is that of power energy/time, as measured in watts (W = J/s, [kg m^2/s^3]).

The wall surfaces where A-Wall-Force is active do not move, but the fluids at $0 \le r < (R - \mathit{\Delta} r)$ relatively travel downstream with a mean velocity V_m. So, it is possible that A-Wall-Force does negative work on the fluid. A-Wall-Power and A-Flow-Power are derived by multiplying both sides of (4.2) by V_m:

$$\begin{aligned} \text{A-Wall-Power} &= 2\pi R(\mathit{\Delta} x)\tau_w V_m = -\pi\mu R^2(\mathit{\Delta} x)(\nabla\times\omega)_x|_{r=R}V_m\\ &= -\mu\mathcal{V}(\nabla\times\omega)_x|_{r=R}V_m, \end{aligned} \tag{4.10}$$

and

$$\text{A-Flow-Power} = \pi R^2(\mathit{\Delta} p)_x V_m = Q(\mathit{\Delta} p)_x, \tag{4.11}$$

where $Q = \pi R^2 V_m$ is the volumetric flux.

ETNA
Kent State University
http://etna.math.kent.edu

4.3. Dimensionless axial wall and flow powers. A-Wall-Power is made dimensionless by dividing by $Q[(1/2)\rho V_m^2]$; see (6.4). In the case of Poiseuille flow for Δx, from (4.7) and (4.10),

$$\text{A-Wall-Power}' = -\frac{2\pi R(\Delta x)[(4\mu V_m)/R]V_m}{Q[(1/2)\rho V_m^2]} = -\frac{64}{\text{Re}}\frac{\Delta x}{D} = -64\Delta X,$$

where $64/\text{Re}$ is the Darcy-Weisbach friction factor for Poiseuille flow.

Similarly, from (4.11),

$$\text{A-Flow-Power}' = \frac{\pi R^2(\Delta p)_x V_m}{Q[(1/2)\rho V_m^2]} = (\Delta p')_x.$$

It is clear from (2.2) that A-Flow-Power′ = A-Wall-Power′ in the Poiseuille region, whereas A-Flow-Power′ $\neq$ A-Wall-Power′ in the developing entrance region. A-Flow-Power′ corresponds to the left-hand term of (2.2).

5. Radial force and power.

In this section, we consider radial forces and powers in the developing entrance region.

5.1. Radial wall and flow forces.

(i) We consider the radial wall shear τ_{rw}. As τ_w is expressed as (4.3), τ_{rw} can be defined by multiplying both sides of (3.5) by $(1/2)R$:

$$\tau_{rw} = -\frac{1}{2}\mu R(\nabla \times \omega)_r\Big|_{r=R} = \frac{1}{2}\mu R\frac{\partial \omega}{\partial x} = \frac{1}{2}R\frac{\partial p}{\partial r} < 0. \tag{5.1}$$

The radial wall force (R-Wall-Force) is expressed from (5.1) as

$$\begin{aligned}\text{R-Wall-Force} &= 2\pi R(\Delta x)\tau_{rw} = -\pi\mu R^2(\Delta x)(\nabla \times \omega)_r = -\mu\mathcal{V}(\nabla \times \omega)_r \\ &= \pi\mu R^2(\Delta\omega)_x\big|_{r=R} = \pi\mu R^2(\omega_{i+1} - \omega_i)\big|_{r=R} < 0.\end{aligned} \tag{5.2}$$

(ii) R-Wall-Force must exert an equal radial flow force (R-Flow-Force) on the fluid in radial direction resulting in the radial pressure drop $(\Delta p)_{wc}$. Then R-Flow-Force is expressed for Δx as

$$\text{R-Flow-Force} = 2\pi(R - \Delta r)(\Delta x)(\Delta p)_{wc} \approx 2\pi R\Delta x(\Delta p)_{wc} < 0. \tag{5.3}$$

Thus

$$\tau_{rw} \approx (\Delta p)_{wc} \qquad \text{and} \qquad \text{R-Wall-Force} \approx \text{R-Flow-Force}. \tag{5.4}$$

(iii) Accordingly, from (3.3), (5.2), and (5.3), it is possible to assume the following process for the acceleration of a fluid in axial direction:

(a) R-Wall-Force on the wall exerts an equal force R-Flow-Force on the fluid in the radial direction by Newton's Second Law of Motion.

(b) R-Wall-Force and R-Flow-Force cause a fluid near the wall to move towards the centerline in the radial direction, as displayed in Figure 2.4, resulting in an increase in kinetic energy; cf. Section 6.1.

(c) An increase in kinetic energy means that the pressure of the fluid is transformed into an increase in kinetic energy of the fluid, as can be seen form the first term on the right-hand side of (3.3). R-Flow-Force shows the result of this change.

(d) R-Flow-Force shows that the pressure on the centerline is higher than that on the wall. As explained in (b) above, however, the fluid near the centerline does not move towards the wall.

(e) Thus R-Wall-Force and R-Flow-Force act as acceleration forces together with the continuity equation. Hence, the onset of the transition should depend on whether or not the acceleration power provided by R-Wall-Force exceeds a required value of ΔKE flux.

5.2. Radial flow work. R-Wall-Force yields a radial velocity v and a pressure drop $(\Delta p)_{wc}$ in the radial direction. Using the pressure drop, the radial flow work (R-Flow-Work) done on a fluid by R-Wall-Force is considered.

Here, on the basis of thermodynamics [14], the variation of the enthalpy H with pressure p at a fixed temperature can be obtained from the definition

$$H \equiv U_{int} + p\mathcal{V},$$

where U_{int} is the internal energy and $\mathcal{V}$ is the volume. For most solids and liquids, at a constant temperature the internal energy $U_{int}(T, \mathcal{V})$ does not change since

$$dU_{int} = \left(\frac{\partial U_{int}}{\partial T}\right)_{\mathcal{V}} dT + \left(\frac{\partial U_{int}}{\partial \mathcal{V}}\right)_{T} d\mathcal{V} = 0,$$

where T is the temperature. Since the change in volume is rather small unless changes in pressure are very large, a change in enthalpy ΔH resulting from a change in pressure Δp can be approximated by

$$\Delta H \approx \Delta(p\mathcal{V}) \approx p\Delta\mathcal{V} + \mathcal{V}\Delta p \approx \mathcal{V}(\Delta p). \tag{5.5}$$

Equation (5.5) can be applied to incompressible flow as well. R-Flow-Work is expressed from (5.5) as

$$\text{R-Flow-Work} = \mathcal{V}(\Delta p)_{wc} = \pi R^2(\Delta x)(\Delta p)_{wc}. \tag{5.6}$$

Note that the dimension of $\mathcal{V}(\Delta p)_{wc}$ is physically equivalent to energy, and by multiplying by frequency (the inverse of the period $\omega|_{r=R}$), the physical dimension of $\mathcal{V}(\Delta p)_{wc}(\omega|_{r=R})$ becomes power; see (5.12).

5.3. Radial flow power.

(i) We begin by calculating the work done on the fluid from (5.6) for the space between x_i and x_{i+1}, Δx, as seen in Figure 2.4. The volume $\mathcal{V}$ on which R-Wall-Force acts is simply expressed as

$$\mathcal{V} = \pi R^2 \Delta x. \tag{5.7}$$

Next, the pressure drop in the radial direction is approximated by the mean difference in pressure between x_i and x_{i+1},

$$(\Delta p_i)_{wc} = \frac{1}{2}[(p_{i,J0} + p_{i+1,J0}) - (p_{i,1} + p_{i+1,1})]. \tag{5.8}$$

(ii) The period during which R-Wall-Force acts on the flow passing along $\omega_{i,J0}$ and $\omega_{i+1,J0}$ on the wall is considered. The period $\Delta t^*(i)$ may be given by dividing the axial mesh space Δx by the mean velocity at two points $(i, J1)$ and $(i+1, J1)$,

$$\Delta t^*(i) = \frac{\Delta x}{(1/2)(u_{i,J1} + u_{i+1,J1})} \approx \frac{\Delta x}{u_{i+1/2,J1}} \cdot$$

ETNA
Kent State University
http://etna.math.kent.edu

However, if this $\Delta t^*(i)$ is the correct period, an inconsistency is encountered. Three simple cases are considered as examples to illustrate this inconsistency.

(a) First, if the mesh aspect ratio is $\Delta x = 2\Delta r$ $(m = 2)$, as observed in Figure 2.4, where Δx is constant, then R-Flow-Work(a) and R-Flow-Power(a) can be expressed as

$$\text{R-Flow-Work}(a) = \mathcal{V}(\Delta p)_{wc}, \tag{5.9}$$

$$\text{R-Flow-Power}(a) = \frac{\mathcal{V}(\Delta p)_{wc}}{\Delta x / u_{i+1/2,J1}} = \frac{\mathcal{V}(\Delta p)_{wc}\, u_{i+1/2,J1}}{2\Delta r}.$$

(b) Next, if Δx and $\mathcal{V}$ are equally divided into two parts, then $\Delta r + \Delta r = \Delta x$ and $\mathcal{V}1 + \mathcal{V}2 = \mathcal{V}$. R-Flow-Work$(b)$ in $\mathcal{V}$ is calculated by adding the work in $\mathcal{V}1$ and the work in $\mathcal{V}2$,

$$\text{R-Flow-Work}(b) = \mathcal{V}1(\Delta p1)_{wc} + \mathcal{V}2(\Delta p2)_{wc} \approx \mathcal{V}(\Delta p)_{wc}. \tag{5.10}$$

R-Flow-Power(b) in $\mathcal{V}$ is calculated by adding the power in $\mathcal{V}1$ and the power in $\mathcal{V}2$,

$$\text{R-Flow-Power}(b) = \frac{\mathcal{V}1(\Delta p1)_{wc}}{\Delta r / u_{i+1/4,J1}} + \frac{\mathcal{V}2(\Delta p2)_{wc}}{\Delta r / u_{i+3/4,J1}} \approx \frac{\mathcal{V}(\Delta p)_{wc}\, u_{i+1/2,J1}}{\Delta r}$$

$$\approx 2\text{R-Flow-Power}(a),$$

assuming that $(\Delta p1)_{wc} \approx (\Delta p2)_{wc} \approx (\Delta p)_{wc}$ and $u_{i+1/4,J1} \approx u_{i+3/4,J1} \approx u_{i+1/2,J1}$. From (5.9) and (5.10), R-Flow-Work(a) equals R-Flow-Work(b). Comparing R-Flow-Power(a) and (b), however, R-Flow-Power(b) is two times R-Flow-Power(a), although the volume and position are the same.

(c) In numerical calculations, usually $\Delta x = m\Delta r$ $(m = 1, 2, 3, \ldots)$. To avoid the inconsistency between (a) and (b) above, the following period is required for a general mesh system of $\Delta x = m\Delta r$:

$$\Delta t_i = \frac{\Delta r}{(1/2)(u_{i,J1} + u_{i+1,J1})} \approx \frac{1}{(1/2)(\omega_{i,J0} + \omega_{i+1,J0})}. \tag{5.11}$$

This period in (5.11) is based on the following assumptions: a rotation of a fluid particle on the wall yields a vortex and a vorticity. Then the curl of vorticity yields R-Wall-Force from (5.2). The diameter of vorticities on the wall is Δr. Accordingly, R-Wall-Force is produced between two continuous vortexes or per Δr.

(iii) R-Flow-Power is derived from (5.7), (5.8), and (5.11):

$$\text{R-Flow-Power} = \pi R^2 \Delta x (\Delta p)_{wc}\, \omega|_{r=R} = \mathcal{V}(\Delta p)_{wc}\, \omega|_{r=R}. \tag{5.12}$$

5.4. Radial wall work and wall power.

(i) The radial wall work (R-Wall-Work) approximately equals R-Flow-Work. From (3.5), (5.1), (5.4), and (5.6), R-Wall-Work can be expressed from R-Flow-Work by replacing $(\Delta p)_{wc}$ with $-(1/2)\mu R(\nabla \times \omega)_r|_{r=R}$:

$$\text{R-Wall-Work} = \pi R^2 (\Delta x)\tau_{rw} = -\frac{1}{2}\pi\mu R^3 (\Delta x)(\nabla \times \omega)_r|_{r=R} = \frac{1}{2}\pi\mu R^3 (\Delta\omega)_x|_{r=R}.$$

(ii) The radial wall power (R-Wall-Power) is obtained by multiplying R-Wall-Work by the vorticity $\omega|_{r=R}$:

$$\text{R-Wall-Power} = \frac{1}{2}\pi\mu R^3 \omega(\Delta\omega)_x|_{r=R}. \tag{5.13}$$

Equation (5.13) approximately equals (5.12):

$$\text{R-Wall-Power} \approx \text{R-Flow-Power}.$$

ETNA
Kent State University
http://etna.math.kent.edu

6. A criterion for determining $\mathbf{R_c}$.

6.1. Kinetic energy flux.

(i) Consider the kinetic energy flux (KE flux) at the inlet. The KE flux varies with inlet shapes such as bell-mouths and with radial velocities. If the velocity profile is the mean velocity V_m only, then the kinetic energy flux across the inlet is given by

$$\text{KE flux}_{\text{Mean}} = \int_0^R (2\pi r dr) V_m \left(\frac{1}{2}\rho V_m^2\right) = \frac{1}{8}\pi\rho D^2 V_m^3 = Q\left(\frac{1}{2}\rho V_m^2\right). \tag{6.1}$$

Note that the physical dimension of KE flux is that of power. In Hagen-Poiseuille flow, the axial velocity distribution is given by (4.4), and the kinetic energy flux of Hagen-Poiseuille flow is

$$\text{KE flux}_{\text{Poiseuille}} = \int_0^R (2\pi r dr)\left(\frac{1}{2}\rho\right)\left\{2V_m\left[1-(\frac{r}{R})^2\right]\right\}^3 dr = 2Q\left(\frac{1}{2}\rho V_m^2\right). \tag{6.2}$$

Let the kinetic energy flux of a fluid at the pipe inlet be KE $\text{flux}_{\text{Inlet}}$. Then, the ΔKE flux is expressed as

$$\Delta\text{KE flux} = \text{KE flux}_{\text{Poiseuille}} - \text{KE flux}_{\text{Inlet}}.$$

(ii) In numerical calculations, dimensionless variables denoted with a prime ($'$) are used:

$$\begin{aligned} &x' = \frac{x}{D} \quad r' = \frac{r}{D}, \quad \omega' = \frac{\omega}{V_m/D}, \quad p' = \frac{p}{(1/2)\rho V_m^2}, \\ &t' = \frac{V_m}{D}t, \qquad \psi' = \frac{\psi}{D^2 V_m}, \qquad X' = \frac{x}{D\text{Re}}, \end{aligned} \tag{6.3}$$

where t' is the time, ψ' is the stream function, and X' is the axial coordinate. Note that the dimensionless axial coordinate x' (= x/D) is used for the calculations, and X' $(= x/(D\ \text{Re}))$ is used in our figures and tables.

(iii) KE flux and ΔKE flux are made dimensionless by dividing by KE $\text{flux}_{\text{Mean}}$. From (6.1) and (6.2), KE $\text{flux}'_{\text{Mean}}$ = 1 and KE $\text{flux}'_{\text{Poiseuille}}$ = 2. The dimensionless ΔKE flux is given by

$$\Delta\text{KE flux}' = \frac{\text{KE flux}_{\text{Poiseuille}} - \text{KE flux}_{\text{Inlet}}}{\text{KE flux}_{\text{Mean}}} = \frac{\Delta\text{KE flux}}{Q[(1/2)\rho V_m^2]}. \tag{6.4}$$

6.2. Determination of $\mathbf{R_c}$.

(i) It appears likely that laminar–turbulent transition always occurs in the developing entrance region, where flow develops into Hagen-Poiseuille flow. In that case, KE flux increases. On the other hand, there is no R-Wall-Power or ΔKE flux in the Poiseuille region. Hence, it is assumed that R-Wall-Force is a possible cause for the flow development and R-Wall-Power is used for ΔKE flux in the developing region.

Let the total R-Wall-Power be T-R-Wall-Power. Thus, the criteria for determining R_c are

$$|\text{T-R-Wall-Power}| \begin{cases} > \Delta\text{KE flux}, & \text{transition does not occur,} \\ = \Delta\text{KE flux}, & \text{Re} = R_c, \text{ and} \\ < \Delta\text{KE flux}, & \text{transition occurs.} \end{cases} \tag{6.5}$$

(ii) When $|\text{T-R-Wall-Power}| > \Delta$KE flux, the difference between $|\text{T-R-Wall-Power}|$ and ΔKE flux might be maintained in the internal energy of the fluid, restoring to the pressure of the fluid.

ETNA
Kent State University
http://etna.math.kent.edu

(iii) Let the total R-Flow-Power be T-R-Flow-Power. Since R-Flow-Power approximately equals R-Wall-Power, the criterion for determining R_c are also

$$|\text{T-R-Flow-Power}| \begin{cases} > \Delta\text{KE flux}, & \text{transition does not occur,} \\ = \Delta\text{KE flux}, & \text{Re} = R_c, \text{ and} \\ < \Delta\text{KE flux}, & \text{transition occurs.} \end{cases}$$

6.3. Sharp-edged inlet pipe and $\mathbf{R_{c,min}}$.

(i) R_c is $R_{c,min}$ when using a sharp-edged inlet pipe under natural disturbance conditions in a water tank. For a sharp-edged pipe, it is assumed that KE $\text{flux}_{\text{Inlet}}$ = KE $\text{flux}_{\text{Mean}}$. ΔKE flux$'$ is calculated from (6.1), (6.2), and (6.4) as

$$\Delta\text{KE flux}' = \frac{2Q[(1/2)\rho V_m^2] - Q[(1/2)\rho V_m^2]}{Q[(1/2)\rho V_m^2]} = 1. \tag{6.6}$$

If KE $\text{flux}_{\text{Inlet}} \neq$ KE $\text{flux}_{\text{Mean}}$, then ΔKE flux$' \neq 1$.

(ii) For a sharp-edged inlet pipe, R-Wall-Power$'$ is reduced from (5.13) to

$$\text{R-Wall-Power}' = \frac{(1/2)\pi\mu R^3\omega(\Delta\omega)_x}{Q[(1/2)\rho V_m^2]} = \left.\frac{\omega'(\Delta\omega)'_x}{2\text{Re}}\right|_{r=R},$$

and

$$|\text{T-R-Wall-Power}'| = \frac{1}{2\text{Re}}\sum_{i=2}^{I1} |\omega'(\Delta\omega)'_x|_{r=R}\,, \tag{6.7}$$

where if $I1(= I0 - 1)$ indicates the Poiseuille region, then $\omega'|_{r=R} = 8$ from (4.6) and (6.3).

If $|\text{T-R-Wall-Power}'| = 1$, then $R_{c,min}$ is obtained from (6.7) as

$$\text{Re} = R_{c,min} = \frac{1}{2}\sum_{i=2}^{I1} |\omega'(\Delta\omega)'_x|_{r=R}\,. \tag{6.8}$$

It is noted [27] that "Equations (6.7) and (6.8) show a possible answer to why Re is the primary parameter for laminar-turbulent transition in pipe flow."

(iii) The dimensionless R-Flow-Power is obtained from (5.12) as

$$|\text{R-Flow-Power}'| = \frac{|\pi R^2(\Delta x)\omega(\Delta p)_{wc}|}{Q[(1/2)\rho V_m^2]} = |(\Delta x')\omega'(\Delta p')_{wc}|,$$

and

$$|\text{T-R-Flow-Power}'| = \sum_{i=2}^{I1} |(\Delta x')\omega'(\Delta p')_{wc}|. \tag{6.9}$$

If $|\text{T-R-Flow-Power}'| = 1$, then Re = $R_{c,min}$.

Equations (6.7) and (6.9) can be solved by an interpolation method with varying Re.

6.4. Stability of Poiseuille flow.

(i) We consider the question why Poiseuille flow is stable by using the shear stress $\mu(du/dr)$. Let the shear forces exerted on a fluid by shear stresses at r and $(r + \Delta r)$ for Δx be τ-force$_1$ and τ-force$_2$, respectively. From (4.4),

$$\tau\text{-force}_1 = (2\pi r\Delta x)\mu\frac{du}{dr} = -\frac{8\pi\mu V_m \Delta x(r^2)}{R^2},$$

ETNA
Kent State University
http://etna.math.kent.edu

$$\tau\text{-force}_2 = [2\pi(r+\mathit{\Delta} r)\mathit{\Delta} x]\mu\frac{du}{dr} = -\frac{8\pi\mu V_m \mathit{\Delta} x(r+\mathit{\Delta} r)^2}{R^2}\,.$$

Then the shear force per unit volume is expressed by subtracting τ-force$_1$ from τ-force$_2$ resulting in the constant axial pressure difference:

$$\begin{aligned}\frac{\tau\text{-force}_2-\tau\text{-force}_1}{2\pi r\mathit{\Delta} r\mathit{\Delta} x} &= -\frac{8\mu V_m}{R^2} = -\frac{32\mu V_m}{D^2}\frac{(1/2)\rho V_m^2}{(1/2)\rho V_m^2}\\ &= -\frac{64\mu}{\rho D V_m}\frac{1}{D}\left(\frac{1}{2}\rho V_m^2\right) = -\frac{64}{\mathrm{Re}}\frac{1}{D}\left(\frac{1}{2}\rho V_m^2\right) = \frac{(\mathit{\Delta} p)_x}{\mathit{\Delta} x}\,.\end{aligned} \tag{6.10}$$

From (6.10), the Darcy-Weisbach friction factor $f = 64/\mathrm{Re}$ in (2.2) is obtained.

Thus the constant shear force of $(-8\mu V_m/R^2)$ is active across the radius in the entire Poiseuille region, so that transition to turbulence will not occur in the Poiseuille region.

(ii) Our earlier calculated results of the axial velocity development [25] show that the velocity distribution is concave in the central portion for $X < 0.0002$ at Re = 2000 and appears approximately flat in the central portion for $0.0003 < X < 0.004$. It is clear from the calculated results that the magnitude of shear force per unit volume near the wall is larger than that in the central portion resulting in a difference in energy of the fluid in the radial direction. Therefore, differences in the shear force and in the energy of a fluid in radial direction trigger a transition to turbulence in the developing entrance region.

7. Calculation of $\mathbf{R_{c,min}}$.

Part of this section refers to our earlier calculations [10]. The notational primes denoting dimensionless expressions are hereafter elided for simplicity.

7.1. Governing equations. We introduce the stream function and vorticity formulae in two-dimensional cylindrical coordinates for the governing equations to avoid the explicit appearance of the pressure term. Accordingly, the velocity fields are determined without any assumptions concerning pressure. Subsequently, the pressure distribution is calculated using values of the velocity fields.

Let ψ be the stream function. The dimensionless transport equation for the vorticity ω is expressed as

$$\frac{\partial\omega}{\partial t} - \frac{1}{r}\frac{\partial\psi}{\partial x}\frac{\partial\omega}{\partial r} + \frac{1}{r}\frac{\partial\psi}{\partial r}\frac{\partial\omega}{\partial x} + \frac{\omega}{r^2}\frac{\partial\psi}{\partial x} = \frac{1}{\mathrm{Re}}\left\{\frac{\partial}{\partial r}\left[\frac{1}{r}\frac{\partial(r\omega)}{\partial r}\right] + \frac{\partial^2\omega}{\partial x^2}\right\}\,.$$

The Poisson equation for ω is derived from the definition of ω, i.e.,

$$-\,\omega = \nabla^2\psi = \frac{\partial}{\partial r}\left(\frac{1}{r}\frac{\partial\psi}{\partial r}\right) + \frac{\partial^2}{\partial x^2}\left(\frac{\psi}{r}\right),$$

where only the angular (θ) component of ω in a two-dimensional flow field is effective, and thus ω denotes ω_θ. The axial velocity u and radial velocity v are defined as derivatives of the stream function, i.e.,

$$u = \frac{1}{r}\,\frac{\partial\psi}{\partial r}, \qquad v = -\,\frac{1}{r}\,\frac{\partial\psi}{\partial x}. \tag{7.1}$$

The pressure can be calculated from the steady-state form of the N-S equations. The pressure distribution for the x-partial derivative is

$$\frac{\partial p}{\partial x} = -2\left(u\frac{\partial u}{\partial x} + v\frac{\partial u}{\partial r}\right) + \frac{2}{\mathrm{Re}}\left(\frac{\partial^2 u}{\partial x^2} + \frac{1}{r}\frac{\partial u}{\partial r} + \frac{\partial^2 u}{\partial r^2}\right), \tag{7.2}$$

and that for the r-partial derivative is

$$\frac{\partial p}{\partial r} = -2\left(u\frac{\partial v}{\partial x} + v\frac{\partial v}{\partial r}\right) + \frac{2}{\text{Re}}\left(\frac{\partial^2 v}{\partial x^2} + \frac{1}{r}\frac{\partial v}{\partial r} - \frac{v}{r^2} + \frac{\partial^2 v}{\partial r^2}\right). \tag{7.3}$$

Since u and v are known at every point from (7.1), a smooth pressure distribution that satisfies both (7.2) and (7.3) is calculated using the Poisson equation for the pressure [20],

$$\nabla^2 p = \frac{\partial^2 p}{\partial x^2} + \frac{\partial^2 p}{\partial r^2} + \frac{1}{r}\frac{\partial p}{\partial r} = -2\left[\left(\frac{\partial v}{\partial r}\right)^2 + 2\frac{\partial u}{\partial r}\frac{\partial v}{\partial x} + \left(\frac{\partial u}{\partial x}\right)^2 + \frac{v^2}{r^2}\right]. \tag{7.4}$$

Initial values are determined using (7.2), and then (7.4) is used to obtain better solutions.

7.2. Numerical method and the mesh system. The finite difference equations for both the stream function-vorticity and the pressure are solved by the Gauss-Seidel iterative method. This computational scheme uses the Forward-Time, Centered-Space (FTCS) method. The scheme has second-order accuracy in the space variables and first-order accuracy in time. The rectangular mesh system used is schematically illustrated in Figure 2.4, where $I0$ and $J0$ are the maximum coordinates for axial and radial mesh points, respectively, and $I1 = I0 - 1$ and $J1 = J0 - 1$. $J0$ is located on the wall, and $J1$ is located at the wall.

To calculate R-Wall-Power and R-Flow-Power, two mesh systems (b) and (c) are used for four Reynolds numbers, 1000, 2000, 4000, and 10,000 (cf. [10]): (b) $I0$ = 1001, $J0$ =51, ΔX = 0.00002, $\Delta x = \text{Re}\Delta X$, and max X = 0.02, and (c) $J0$ =101, with other parameters the same as for (b).

7.3. Vorticity on the wall. The vorticity boundary condition on no-slip walls is derived from (3.1) as $\omega|_{r=R} = -du/dr$. A three-point, one-sided approximation for (3.1) is used to maintain second-order accuracy,

$$\omega|_{r=R} = \omega_{i,J0} \approx -\frac{3u_{i,J0} - 4u_{i,J1} + u_{i,J2}}{2\Delta r} = \frac{4u_{i,J1} - u_{i,J2}}{2\Delta r}. \tag{7.5}$$

The boundary conditions for the axial velocity at the pipe inlet ($i = 1$) are approximated as

$$u_{1,j} = 1, \qquad 1 \le j \le J1, \qquad \text{and} \qquad u_{1,J0} = 0. \tag{7.6}$$

Table 7.1 and Figure 7.1 show the vorticities on the wall. Our major conclusions for the vorticity distribution are:

(i) A large value of vorticity may appear at a pipe inlet edge. According to (7.5) and (7.6), $\omega_{1,J0}$ at the pipe inlet is 150 for $J0 = 51$ ($\Delta r = 0.01$) and 300 for $J0 = 101$ ($\Delta r = 0.005$); i.e., if $\Delta r \to 0$, then $\omega_{1,J0} \to \infty$. In the FTCS method, $\omega_{1,J0}$ is not used, so that reasonable values of $\omega|_{r=R}$ can be observed in Table 7.1 and Figure 7.1.

(ii) It is clear from Table 7.1 that for $X \ge 0.00002$, the vorticity on the wall is approximately the same for $J0$ = 51 and 101 but varies somewhat with Re. For $X \ge 0.0001$ the vorticity on the wall is independent of Re and the size of Δr.

7.4. Radial pressure drop along the pipe. A natural transition occurs where X is less than 0.01 experimentally, so the pressure drop for $X \le 0.02$ was calculated. To verify the accuracy of the calculations, the calculated results for the pressure drop are compared with Shapiro's experimental results [24] as displayed in Figure 7.2(a) through (d) (cf. Figures. 7–10 in [10]), where $zz = X$.

ETNA
Kent State University
http://etna.math.kent.edu

TABLE 7.1
Vorticity vs. X and Re, (b) $J0$ = 51 and (c) $J0$ = 101.

X	1000-b	2000-b	4000-b	10000-b	1000-c	2000-c	4000-c	10000-c
0.00002	100.2	83.3	70.3	60.8	112.4	85.0	69.8	59.6
0.00004	66.0	49.8	41.5	38.8	55.6	42.8	37.9	37.3
0.00006	46.7	36.0	32.6	33.5	38.5	32.6	31.5	33.5
0.00008	36.4	30.3	29.6	31.6	31.8	28.9	29.5	31.8
0.0001	31.0	27.7	28.4	30.3	28.4	27.1	28.4	30.4
0.0002	23.1	24.1	25.4	25.8	22.7	24.1	25.5	25.9
0.0005	19.1	20.0	20.2	20.1	19.1	20.1	20.3	20.2
0.001	16.3	16.6	16.6	16.6	16.4	16.7	16.7	16.6
0.005	11.0	11.0	11.0	11.0	11.0	11.0	11.0	11.0
0.01	9.6	9.6	9.6	9.6	9.6	9.6	9.6	9.6
0.02	8.8	8.8	8.8	8.8	8.8	8.8	8.8	8.8

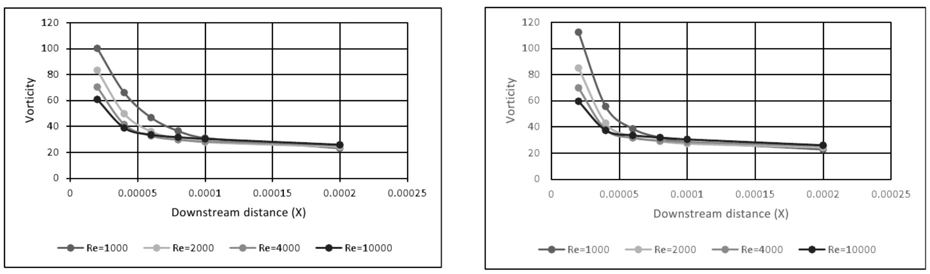

(b) $J0$ = 51

(c) $J0$ = 101

FIG. 7.1. *Vorticity vs. X for Re = 1000, 2000, 4000, and 10,000.*

The major conclusions for the radial pressure distribution are as follows:

(i) From Figure 7.2, the radial pressure difference $|(\Delta p)_{wc}|$ decreases as Re increases; i.e., |R-Flow-Power| drops with Re.

(ii) Consider the above item in detail. So far, three major aspects have been studied regarding phenomena in the entrance region [6]: (a) the pressure difference between any two sections in axial direction, (b) the velocity distribution at any section, and (c) the length of the entrance region L_e. According to many previous investigations, variables such as velocity and pressure distributions become similar and independent of the Reynolds number when they are plotted against the dimensionless distance X (= $x/(D\mathrm{Re})$).

Accordingly, it is important to find variables which decrease in the X coordinate as Re increases since transition occurs as Re increases. For that purpose we identified R-Wall-Force, R-Wall-Power, R-Flow-Force, R-Flow-Work, and R-Flow-Power, presented here for the first time.

(iii) $(\Delta p)_{wc}$ can be used to calculate R-Flow-Power.

(iv) It is necessary to numerically calculate $(\Delta p)_{wc}$ with varying mesh systems and with varying inlet boundary conditions to obtain more precise values of $(\Delta p)_{wc}$.

7.5. Calculation of $\mathbf{R_{c,min}}$. |T-R-Wall-Power| and |T-R-Flow-Power| are obtained from (6.7) and (6.9), respectively, and the calculated results are displayed in Figure 7.3, where the minimum critical Reynolds number $R_{c,min}$ is obtained via linear interpolation.

ETNA
Kent State University
http://etna.math.kent.edu

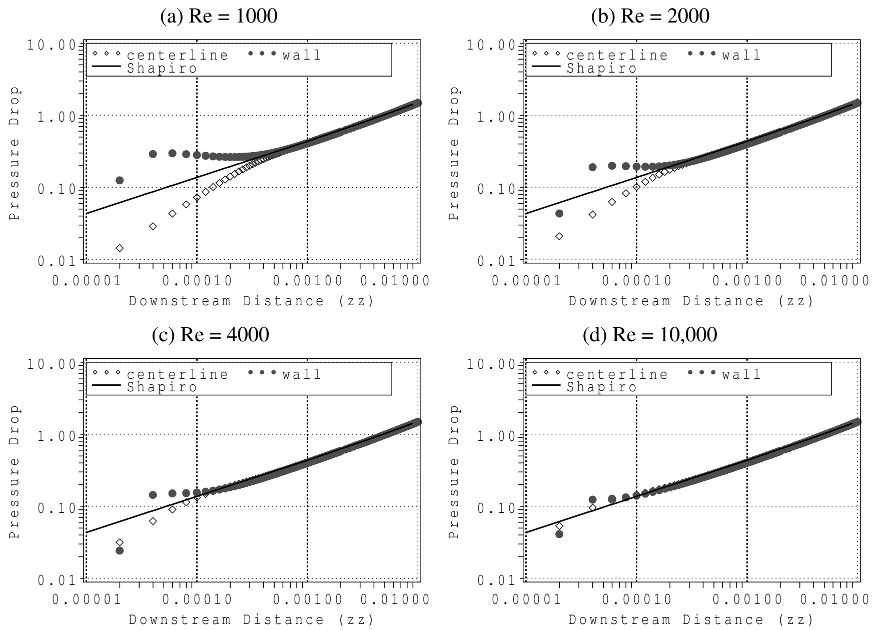

FIG. 7.2. *Difference in pressure drop between on the wall and on the centerline* $(\Delta p)_{wc}$*,* $J0$ *= 101, where* $zz = X = x/(D\,Re)$.

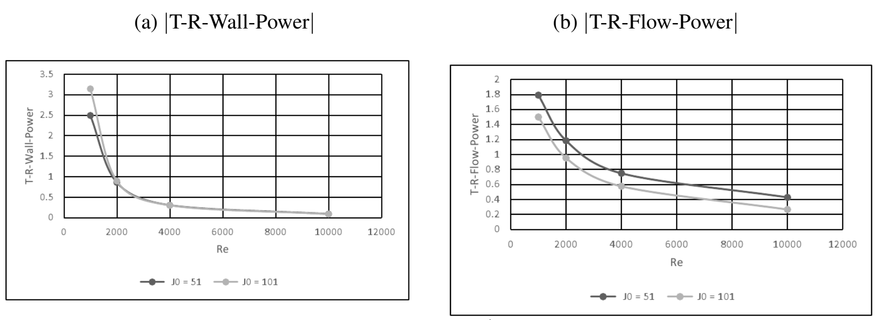

Re-mesh	1000-b	2000-b	4000-b	10000-b	1000-c	2000-c	4000-c	10000-c
TRWP	2.494	0.859	0.305	0.091	3.143	0.895	0.301	0.087
$R_{c,min}$		1910				1950		
TRFP	1.789	1.183	0.747	0.427	1.497	0.952	0.574	0.265
$R_{c,min}$		2840				1910		

FIG. 7.3. $R_{c,min}$ *based on (a) |T-R-Wall-Power| (TRWP) and |T-R-Flow-Power| (TRFP) for mesh systems (b)* $J0$ *= 51 and (c)* $J0$ *= 101.*

For |T-R-Wall-Power| and $J0$ = 51,

$$\frac{R_{c,min} - 1000}{2000 - 1000} = \frac{1 - 2.494}{0.859 - 2.494} \qquad \text{and} \qquad R_{c,min} = 1910.$$

Similarly, $R_{c,min}$ = 1950 for $J0$ = 101. For |T-R-Flow-Power|, $R_{c,min}$ = 2840 for $J0$ = 51, and 1910 for $J0$ = 101.

In the case of |T-R-Wall-Power|, both calculated values of $R_{c,min}$ are close to Reynolds' experimental value of 2050. When using |T-R-Flow-Power|, the calculated value for $J0 = 51$ is somewhat higher than the experimental value, although the value for $J0 = 101$ is close to the

ETNA
Kent State University
http://etna.math.kent.edu

experimental value. Approximations for the pressure field in a pipe needs to be reconsidered in future investigations.

In summary, |T-R-Wall-Power| and |T-R-Flow-Power| vs. ΔKE flux are possible methods for calculating R_c.

8. Discussion of the difference in $\mathbf{R_c}$.

8.1. Difference between $\mathbf{R_{c1,min}}$ and $\mathbf{R_{c2,min}}$. Let the flow state be laminar. It is assumed that ΔKE flux$_{\text{Variance}}$ is the variance from KE flux$_{\text{Mean}}$ if the inlet velocity is not the mean velocity V_m and that ΔKE flux includes the inlet loss K_{inlet} due to inlet disturbances. Accordingly, the required kinetic energy flux for the development into Hagen-Poiseuille flow is described as

$$\begin{aligned}\Delta\text{KE flux} &= \text{KE flux}_{\text{Poiseuille}} - \text{KE flux}_{\text{Inlet}} + K_{\text{Inlet}} \\ &= \text{KE flux}_{\text{Poiseuille}} - (\text{KE flux}_{\text{Mean}} + \Delta\text{KE flux}_{\text{Variance}}) + K_{\text{Inlet}} \\ &= 1 - \Delta\text{KE flux}_{\text{Variance}} + K_{\text{Inlet}},\end{aligned} \tag{8.1}$$

where KE flux$_{\text{Poiseuille}}$ = 2, KE flux$_{\text{Mean}}$ = 1 (see Section 6.1).

There are two possible terms in (8.1) to which the difference between our experimental values $R_{c1,min} \approx 2200$ and $R_{c2,min} \approx 2050$ might be ascribed: ΔKE flux$_{\text{Variance}}$ and K_{Inlet}. Recall from (6.5) that ΔKE flux is equal to |T-R-Wall-Power| when Re is R_c.

First, in the case that ΔKE flux varies and $K_{\text{Inlet}} = 0$, if ΔKE flux is assumed to be inversely proportional to Re around Re = 2000–2300, then ΔKE flux at Re = 2200 is approximated by

$$\Delta\text{KE flux}_{R_{c1,min}} \times 2200 \;=\; \Delta\text{KE flux}_{R_{c2,min}} \times 2050.$$

Then,

$$\Delta\text{KE flux}_{R_{c2,min}} = 1, \quad \Delta\text{KE flux}_{R_{c1,min}} \approx 0.932, \quad \text{and} \quad \Delta\text{KE flux}_{\text{Variance}} \approx 0.068.$$

The velocity distribution for turbulent flow in a pipe is flatter than that for laminar flow. Thus, the value of 0.068 for ΔKE flux$_{\text{Variance}}$ is possible for the difference between $R_{c1,min}$ and $R_{c2,min}$. Figure 8.1(a) conceptually shows the difference between $R_{c1,min}$ and $R_{c2,min}$ in the first case.

Second, if ΔKE flux$_{\text{Variance}} = 0$ and $K_{\text{Inlet}} \neq 0$, then

$$\Delta\text{KE flux}_{R_{c1,min}} \times 2200 \;=\; (\Delta\text{KE flux}_{R_{c2,min}} + K_{\text{Inlet}}) \times 2050.$$

Then,

$$\Delta\text{KE flux}_{R_{c2,min}} = 1, \quad \text{and} \quad K_{\text{Inlet}} \approx 0.073, \quad \Delta\text{KE flux}_{R_{c1,min}} = 1. \tag{8.2}$$

Here, both velocity distributions at the inlet are uniform and ΔKE flux = 1. The assumption of K_{Inlet} = 0.073 causes the difference between $R_{c1,min}$ and $R_{c2,min}$. Exact calculations and experiments will determine which case is operative in future investigations.

8.2. Effects of the bell-mouth entrance on $\mathbf{R_c}$. R-Wall-Power is generated on the walls of a bell-mouth entrance and a pipe, indicating that R-Wall-Power depends upon Re when the entrance shape is fixed. Here, it is considered referring to Figure 8.1(b) why and how R_{c2} is about 5500 for the Be4 bell-mouth entrance with C_b = 6 as displayed in Figure 2.2. Let the average velocity at the bell-mouth inlet end, V_{bell}, be V_m/C_b^2. The increase in kinetic energy

ETNA
Kent State University
http://etna.math.kent.edu

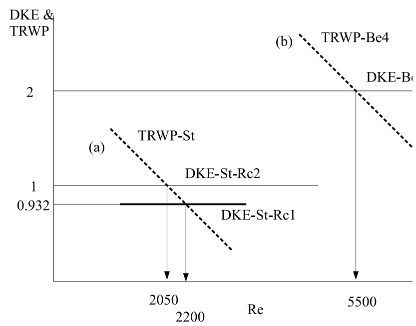

FIG. 8.1. *Two parameters, |T-R-Wall-Power| (TRWP) and ΔKE flux (DKE) to determine R_c: (a) $R_{c1,min}$ = 2200 and $R_{c2,min}$ = 2050 for sharp edged pipe, and (b) $R_{c2} \approx$ 5500 for Be4 bell-mouth entrance with C_b = 6.*

flux between the bell-mouth inlet end and the Poiseuille region is approximated in dimensional form by

$$\Delta \text{KE flux}_{\text{Bell}} \;=\; \frac{\pi}{4}\rho D^2 V_m^3 - \frac{\pi}{8}\rho\frac{1}{C_b^4}D^2V_m^3 \;=\; Q(\frac{1}{2}\rho V_m^2)(2-\frac{1}{C_b^4}). \tag{8.3}$$

The dimensionless form of (8.3) is given by

$$\Delta \text{KE flux}_{\text{Bell}} \;=\; 2-\frac{1}{C_b^4}.$$

From this relation, the ΔKE flux value increases from 1 to 2 as C_b increases.

9. Questions about disturbances.

9.1. Disturbance amplitude.

(i) Flow in the entrance region is sensitive to N-S disturbances, whereas A-L disturbances are required to trigger transition in a Hagen-Poiseuille flow. Hence, are there double disturbance standards for transitions in the entrance flow and Hagen-Poiseuille flow?

(ii) Consider the disturbance loss coefficient. A pipe system has many fitting losses, including entrance shape, bends, elbows, valves, expansions, and contractions. They can be aggregated into a single total system loss using the pressure drop equation (2.2). The pressure drop $\Delta\mathcal{P}$, head loss Δh, and fitting loss coefficient K for a valve, device, or fitting are related by

$$\Delta\mathcal{P} \;=\; K\Big(\frac{1}{2}\rho V_m^2\Big) \;=\; \rho g(\Delta h). \tag{9.1}$$

The loss coefficient K is derived from (9.1) as

$$K = \frac{\Delta\mathcal{P}}{(1/2)\rho V_m^2} = \frac{\Delta h}{V_m^2/(2g)}\,. \tag{9.2}$$

Next, the power dissipation of a valve generating continuous disturbances is considered.

$$\text{Power dissipation} \;=\; Q(\Delta\mathcal{P}) \;=\; QK\Big(\frac{1}{2}\rho V_m^2\Big),$$

where the dimensions are those of power. On the other hand, the energy of a pulse disturbance is given by

$$\text{Energy} \;=\; Q(\Delta t)K\left(\frac{1}{2}\rho V_m^2\right) \;=\; Q(\Delta t)(\rho g \Delta h).$$

To compare the magnitude of a pulse disturbance with that of a continuous disturbance, the width Δt of the pulse disturbance must be a single second so that the integrated magnitude of the pulse becomes power. That is, continuous disturbances are divided into a series of single-second discrete disturbances, and each one-second discrete disturbance is compared with the one-second pulse disturbance using the same units of power. If Δt for a pulse disturbance is less than one second, then the value of Δt can be used as a non-unit weight $\overline{\Delta t}$ of the pulse disturbance.

As a result, the magnitude of disturbances expressed in the dimension of power is given as

$$\text{Disturbance magnitude} \;=\; \begin{cases} QK\left(\frac{1}{2}\rho V_m^2\right), & \text{continuous pulse of } \Delta t \geq 1, \\ Q(\overline{\Delta t})K\left(\frac{1}{2}\rho V_m^2\right), & \text{pulse of } \Delta t < 1. \end{cases}$$

In a pipe system, since Q and $(1/2)\rho V_m^2$ are constant, the disturbance magnitude reduces to a coefficient:

$$\text{Disturbance loss coefficient} \;=\; \begin{cases} K, & \text{continuous pulse of } \Delta t \geq 1, \\ (\overline{\Delta t})K, & \text{pulse of } \Delta t < 1. \end{cases} \tag{9.3}$$

(iii) Consider Hof et al.'s disturbance amplitude [9]. Let $\epsilon = \epsilon(\mathrm{Re})$ denote the minimal amplitude of all finite perturbations that can trigger transition. If ϵ scales with Re according to $\epsilon = O(\mathrm{Re}^{\gamma})$ as $\mathrm{Re} \to \infty$, then what is the value of the exponent γ? Hof et al. obtained $\gamma = -1$ for $2000 < \mathrm{Re} < 18{,}000$ using a single "boxcar" rectangular pulse of fluid, injected tangentially into a flow via a ring of six equally spaced holes, from which the pressure trace of the perturbation was observed. Then, D = 20 mm, Δh = 37 mm H_2O, Δt = 1.2 s (length = $6D$), and V_m = 0.1 m/s at Re ≈ 2000. Thus, the loss coefficient K for the pulse disturbance is calculated from (9.2) and (9.3) as

$$K = \frac{37 \times 10^{-3}}{0.1^2/(2 \times 9.8)} = 72.5.$$

For example, the values of K in a screwed 20-mm-pipe-fitting system are 10 for a glove valve, 0.28 for a gate valve, and 6.1 for an angle valve; cf. [1, Table 1 in ASHRAE Handbook 22.2]. The amplitude of the injected-pulse disturbance of $K = 72.5$ is much larger than that of these valves. Therefore, it is difficult to compare N-S disturbances in the inlet flow and A-L disturbances injected into Hagen-Poiseuille flow.

(iv) What is the magnitude of natural disturbances? The disturbance loss coefficient K_{Dist} may be expressed as

$$K_{\mathrm{Dist}} \;=\; \frac{(V_m + u_m')^2 - V_m^2}{V_m^2}, \tag{9.4}$$

where u_m' is the axial velocity perturbation in V_m.

The perturbations in turbulent flow were observed as $u_c'/V_c \approx 0.035$ for $x/D > 60$, where the subscript 'c' denotes centerline; see [29, Figure 5]. If $u_c'/V_c \approx u_m'/V_m$, then K_{Dist} is obtained from (9.4): $K_{\mathrm{Dist}} \;=\; 1.035^2 - 1 \approx 0.071$. The disturbance loss of K_{Dist} = 0.071 is much less than the value of |T-R-Wall-Power| ≈ 1 around Re = 2000, so that R-Wall-Force can depress disturbed flow and change it into laminar flow.

Accordingly, it may be stated that a possible cause of the onset of transition is the wall effects exerted by R-Wall-Force rather than an oscillation of disturbances.

ETNA
Kent State University
http://etna.math.kent.edu

Conclusions. A definite and fundamental problem of fluid dynamics is to theoretically obtain Reynolds' findings of $R_{c,min} \approx 2050$ and R_{c1} = 12,800 for the transition to turbulence in circular pipe flow. It seems that a transition in circular pipe flows always occurs in the developing entrance region, where the axial velocity distribution develops from an uniform flow at the inlet to the Poiseuille profile, and the kinetic energy of the flow increases, i.e., that a $\varDelta$KE flux exists.

In this paper we have studied this flux by the introduction of R-Wall-Power, which arises due to the radial component of the viscous term (R-Wall-Force) in the Navier-Stokes equations on the wall.

Accordingly, the hypothesized criterion for laminar-turbulent transition can be tersely expressed as follows: transition occurs if and only if |T-R-Wall-Power| $<$ $\varDelta$KE flux. The criterion simply implies that if a pipe flow develops into Hagen-Poiseuille flow, then transition does not occur, and if not, transition occurs.

R-Wall-Power clarified that under natural disturbance conditions, (i) R-Wall-Power and $\varDelta$KE flux are effective only in the entrance region, so that the transition occurs only in the entrance region, (ii) R-Wall-Force is a possible cause of a transition process, (iii) the Reynolds number becomes a critical Reynolds number, i.e., Re = R_c when |T-R-Wall-Power| = $\varDelta$KE flux, and (iv) the R_c value depends upon both the entrance shape and the flow conditions at the inlet. Thus, R_c takes a minimum value of about 2050 only when using a sharp-edged entrance pipe.

Future investigations will be (i) to numerically calculate T-R-Wall-Power with varying mesh systems and with varying inlet boundary conditions, and (ii) to determine why and how R_c takes values of about 5500 and 12,800 when using a bell-mouth entrance.

Acknowledgments. The author wishes to express his sincere appreciation to Professors M. Cohen and M. Honma of the University of Aizu, Dr. K. Shimomukai of SGI Japan, Mr. T. Yanagiya, Professor Emeritus F. Stenger of the University of Utah, and the ETNA referees for encouragement and valuable technical advice.

Appendix A. Notation.

A	=	artificial disturbance condition
Be	=	bell-mouth entrance pipe
C_b	=	contraction ratio (D_b/D)
D	=	pipe diameter
D_b	=	bell-mouth and quadrant-arc inlet diameter
f	=	Darcy-Weisbach friction factor, (2.2)
H	=	enthalpy
i	=	axial point of mesh system
I_0	=	maximum axial mesh point
j	=	radial point of mesh system
J_0	=	maximum radial mesh point
K	=	minor pressure loss
K_{Dist}	=	inlet disturbance loss, (9.4)
K_{Inlet}	=	inlet disturbance loss, (8.2)
L_e	=	dimensionless entrance length $(x_e/(D\text{Re}))$
N	=	natural disturbance condition
p	=	pressure
$\mathcal{P}$	=	pressure $(\mathcal{P} = -p)$
Q	=	volumetric flux $((\pi/4)D^2V_m)$
r	=	radial coordinate; radius of quadrant-arc rounded entrance

R	=	pipe radius
R_c	=	critical Re for laminar–turbulent transition
R_{c1}	=	R_c under S disturbance conditions
R_{c2}	=	R_c under M disturbance conditions
R_{c3}	=	R_c under L disturbance conditions
Re	=	Reynolds number (DV_m/ν)
St	=	sharp-edged entrance pipe
u	=	axial velocity
U_{int}	=	internal energy of a fluid
v	=	radial velocity
V_m	=	mean axial velocity
$\mathcal{V}$	=	volume
x	=	axial coordinate
x'	=	dimensionless axial coordinate (x/D)
x_e	=	entrance length
x_t	=	transition length from inlet
X	=	dimensionless axial coordinate ($x/(D\mathrm{Re})$)
θ	=	cylindrical coordinate
μ	=	viscosity coefficient
ν	=	kinematic viscosity (μ/ρ)
ρ	=	density
τ_w	=	wall shear, (4.1)
τ_{rw}	=	radial wall shear, (5.1)
ω	=	vorticity
$\varDelta$KE flux	=	difference in kinetic energy flux, (6.4)

REFERENCES

[1] ASHRAE HANDBOOK COMMITTEE, *ASHRAE Handbook of Fundamentals (SI)*, ASHRAE, Atlanta, 2009.

[2] K. AVILA, D. MOXEY, A. DE LOZAR, M. AVILA, D. BARKELEY, AND B. HOF, *The onset of turbulence in pipe flow*, Science, 333 (2011), pp. 192–196.

[3] R. P. BENEDICT, *Fundamentals of Pipe Flow*, Wiley, New York, 1980.

[4] B. ECKHARDT, *Turbulence transition in pipe flow: 125th anniversary of the publication of Reynolds' paper*, Philos. Trans. R. Soc. A, 367 (2009), pp. 449–455.

[5] R. W. FOX AND A. T. MCDONALD, *Introduction to Fluid Mechanics*, Wiley, New York, 1994.

[6] S. GOLDSTEIN, *Modern Developments in Fluid Dynamics, Vol. I*, Dover, New York, 1965.

[7] R. A. GRANGER, *Fluid Mechanics*, Dover, New York, 1995.

[8] R. W. HANKS, J. M. PETERSON, AND C. NARVAEZ, *The influence of inlet flow disturbances on transition of Poiseuille pipe flow*, AIChE J., 25 (1979), pp. 181–183.

[9] B. HOF, A. JUEL, AND T. MULLIN, *Scaling of the turbulence transition threshold in a pipe*, Phys. Rev. Lett., 91 (2003), 244502 (4 pages).

[10] H. KANDA, *Computerized model of transition in circular pipe flows. Part 2. Calculation of the minimum critical Reynolds number*, in Proc. ASME Fluids Engeneering Division-1999, D. E. Stock, ed., ASME FED-Vol. 250, ASME, New York, 1999, pp. 197–204.

[11] ———, *Laminar-turbulent transition: Calculation of minimum critical Reynolds number in channel flow,* in Kyoto Conference on the Navier-Stokes Equations and their Applications, Y. Giga, H. Kozono, H. Okamoto, and Y. Shibata, eds., RIMS Kokyuroku Bessatsu B1, RIMS, Kyoto, 2007, pp. 199–217.

[12] H. KANDA AND T. YANAGIYA, *Hysteresis curve in reproduction of Reynolds' color-band experiments*, J. Fluids Engrg., 130 (2008), 051202 (10 pages).

[13] R. R. KERSWELL, *Recent progress in understanding the transition to turbulence in a pipe*, Nonlinearity, 18 (2005), pp. R17–R44.

[14] D. KONDEPUDI AND I. PRIGOGINE, *Modern Thermodynamics*, Wiley, Chichester, 1998.

[15] R. J. LEITE, *An experimental investigation of the stability of Poiseuille flow*, J. Fluid Mech., 5 (1959), pp. 81–96.

[16] E. R. LINDGREN, 1957, *The transition process and other phenomena in viscous flow*, Ark. Fys., 12 (1957),

pp. 1–169.

[17] T. MULLIN AND J. PEIXINHO, *Transition to turbulence in pipe flow*, J. Low Temp. Phys., 145 (2006), pp. 75–88.

[18] R. L. PANTON, *Incompressible Flow*, Wiley, New York, 1984.

[19] O. REYNOLDS, *An experimental investigation of the circumstances which determine whether the motion of water shall be direct or sinuous, and of the Law of resistance in parallel channels*, Philos. Trans. Royal Soc. London, 174 (1883), pp. 935–982.

[20] P. J. ROACHE, *Fundamentals of Computational Fluid Dynamics*, Hermosa, Albuquerque, 1998.

[21] L. SCHILLER, *Experimentelle Untersuchungen zum Turbulenzproblem*, Z. Angew. Math. Mech., 1 (1921), pp. 436–444.

[22] T. M. SCHNEIDER AND B. ECKHARDT, *Edge states intermediate between laminar and turbulent dynamics in pipe flow*, Philos. Trans. R. Soc. A, 367 (2009), pp. 577–587.

[23] R. K. SHAH AND A. L. LONDON, *Laminar Flow Forced Convection in Ducts*, Academic Press, New York, 1978.

[24] A. H. SHAPIRO, R. SHIGEL, AND S. J. KLINE, *Friction factor in the laminar entry region of a smooth tube*, in Proc. 2nd U.S. National Congress of Applied Mathematics, ASME, New York, 1954, pp. 733–741.

[25] K. SHIMONUKAI AND H. KANDA, *Numerical study of normal pressure distribution in entrance pipe flow*, Electron. Trans. Numer. Anal., 30 (2008), pp. 10–25.
http://etna.mcs.kent.edu/vol.30.2008/pp10-25.dir

[26] S. TANEDA, *Gazou-kara Manabu Ryutai Rikigaku* (in japanese) (Fluid Dynamics Studied from Images), Asakura Shoten, Tokyo, 1993.

[27] F. M. WHITE, *Fluid Mechanics*, McGraw-Hill, New York, 1999.

[28] I. J. WYGNANSKI AND F. H. CHAMPAGNE, *On transition in a pipe. Part 1. The origin of puffs and slugs and the flow in a turbulent slug*, J. Fluid Mech., 59 (1973), pp. 281–335.

[29] E.-S. ZANOUN, M. KITO, AND C. EGBERS, *A study on flow transition and development in circular and rectangular ducts*, J. Fluids Engrg., 131 (2009), 061204 (10 pages).